Supplementary data -

Here we show the locations of two additional areas (CC′ and DD′) where the AVO analyses were conducted to identify the base of the hydrate stability zone.

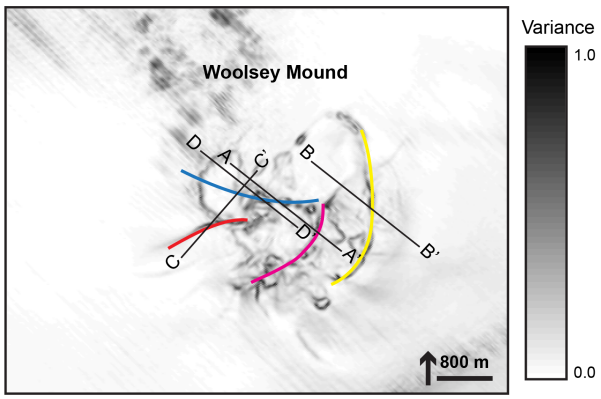

Figure S1. Map view of two additional areas (CC′ and DD′) targeted for the base of the hydrate stability zone identification using AVO analysis. The colored lines represent the master faults.

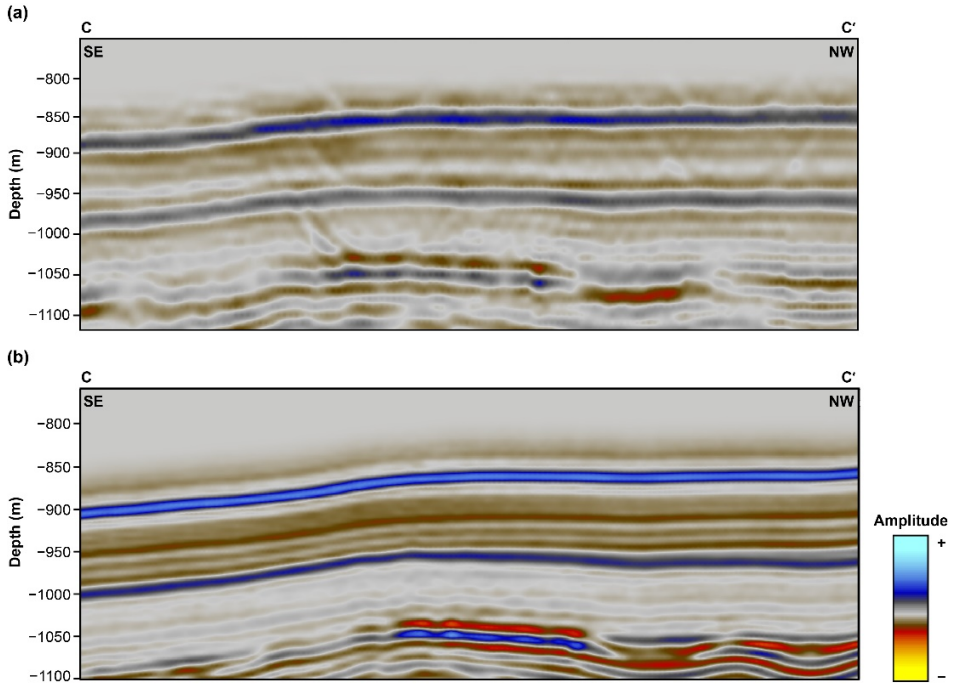

Figure S2. The targeted bright spot. a) bright spot at Inline 20389 from 2010 data and b) bright spot at inline 20389 from 2014 data. These shallow negative polarity amplitude anomalies are hypothesized to represent the boundary separating the hydrate-bearing sediments above from free gas-bearing sediments below.

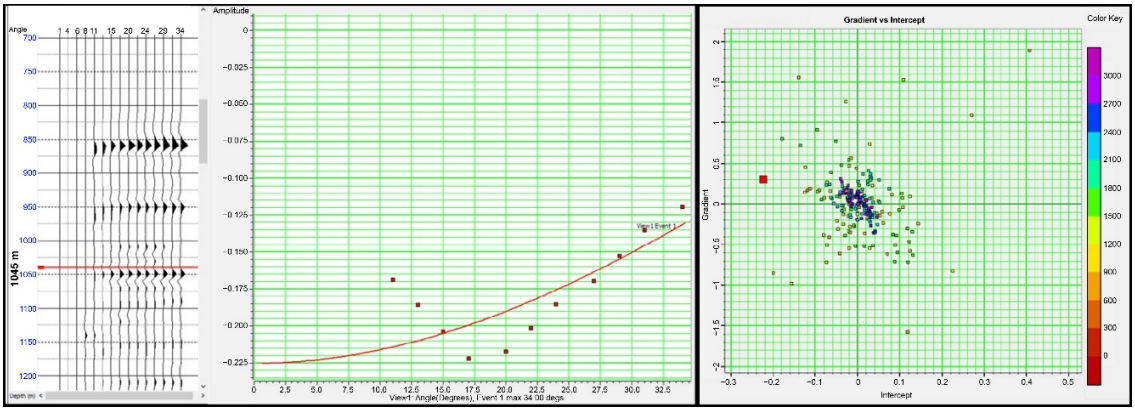

Figure S3. The AVO gradient curve and associated crossplot of 2010 data at CC′. The targeted event, which occurs at 1045 m and is in the second quadrant, exhibits decreasing amplitude with increasing offset.

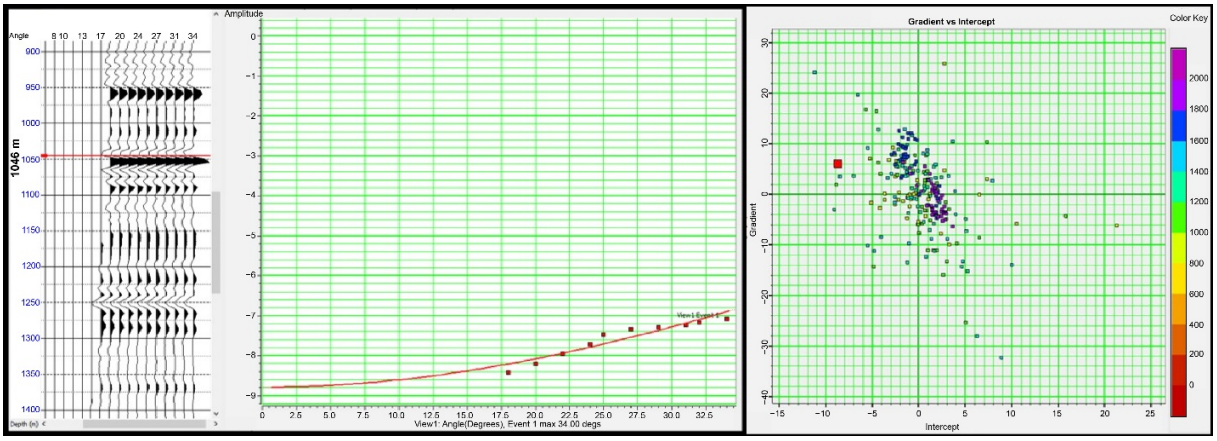

Figure S4. The AVO gradient curve and associated crossplot of 2014 data at CC′. The targeted event, which occurs at 1046 m and is in the second quadrant, exhibits decreasing amplitude with increasing offset.

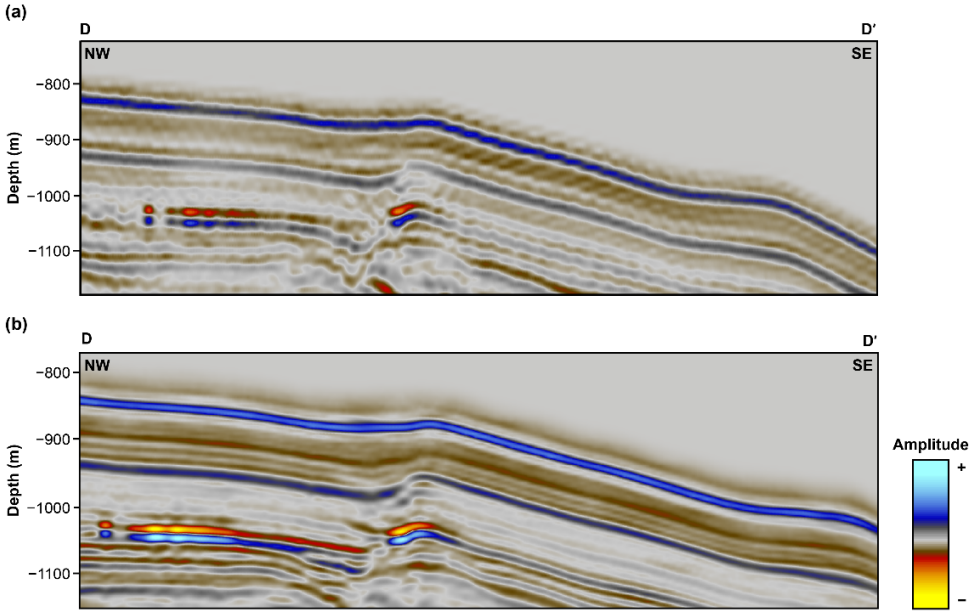

Figure S5. The targeted bright spot. a) bright spot at Inline 11820 from 2010 data and b) bright spot at inline 11820 from 2014 data. These shallow negative polarity amplitude anomalies are hypothesized to represent the boundary separating the hydrate-bearing sediments above from free gas-bearing sediments below.

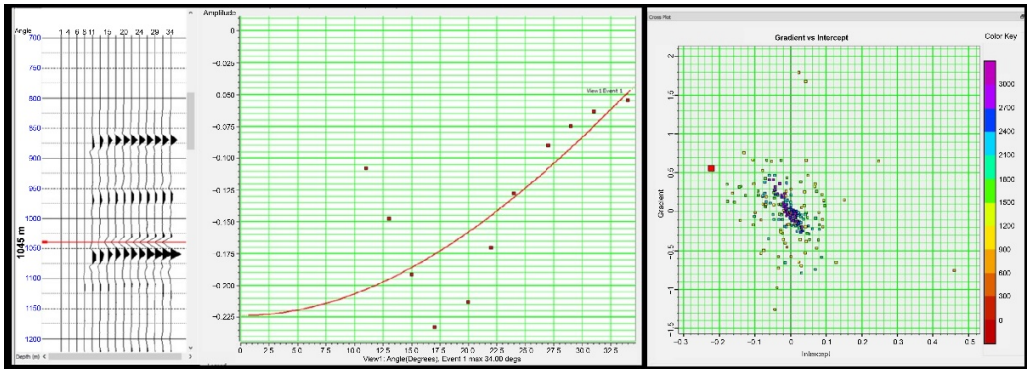

Figure S6. The AVO gradient curve and associated crossplot of 2010 data at DD'. The targeted event, which occurs at 1045 m and is in the second quadrant, exhibits decreasing amplitude with increasing offset.

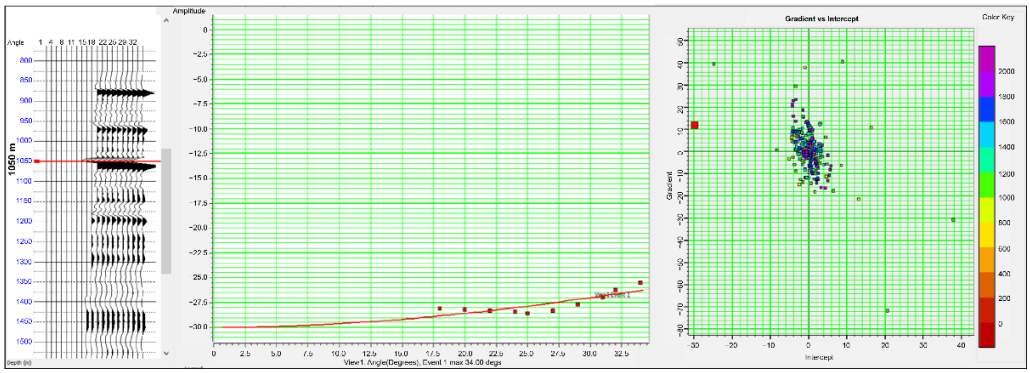

Figure S7. The AVO gradient curve and associated crossplot of 2014 data at DD′. The targeted event, which occurs at 1050 m and is in the second quadrant, exhibits decreasing amplitude with increasing offset.